Mechanics & Industry **16**, 302 (2015)

DOI: 10.1051/meca/2015001
www.mechanics-industry.org

Mechanics & Industry

Surface texturing effect comparative analysis in the hydrodynamic journal bearings

Nacer Tala-Ighil[1,a] and Michel Fillon[2]

[1] Welding and NDT Research Centre (CSC), BP 64, Cheraga, Algeria
[2] Institute Pprime, CNRS, University of Poitiers, ENSMA, Poitiers, France

Received 25 May 2014, Accepted 23 November 2014

Abstract – The journal bearing is a complex system with high film convergence and with cavitation hydrodynamic phenomena. The surface texturation influence study on journal bearing performances requires unavoidably experimental investigations followed by a numerical modelling of the problem. This work consists in modellization and understanding of the journal bearing characteristics in both cases of presence or absence of textures onto the bearing surface. The finite difference method is used as numerical approach in the analysis. The textured bearing performance enhancement passes essentially by an improvement of a minimum film thickness, a maximum pressure and a friction torque through an appropriate surface texture geometry and appropriate texture distribution on the contact surface. It is found that the simulations results are in good concordance with litteratures. The texture area position on the bearing surface is the primary endpoint for journal bearing performance enhancement. The best design of textured area depends strongly on the geometrical parameters and the journal bearing operating conditions.

Key words: Journal bearings / Reynolds equation / hydrodynamic lubrication / Stribeck curve / texture

1 Introduction

Nowadays, there is a strong need to make machines more efficient by looking for power losses and trying to reduce them. The most important losses in a machine come from the bearings [1]. These bearings have several advantages such as low friction and wear, good heat dissipation through the oil and noise and vibrations reduction. The bearing temperature field and pressure field are considerably influenced by the journal bearing parameters [2]. Their lubrication is really important because the contact between surfaces would cause rapid wear [3]. The deterministic roughness that is known as surface texture was introduced deliberately on the bearings using micro-fabrication techniques. Surface texturing is claiming progressively more attention and is expected to be a major component in future bearing structure design as demonstrated by the authors [4, 5]. Patterned or artificially textured surfaces have been studied extensively for many applications, particularly in rotating machinery [6, 7]. Just recently, such textures were engineered in order to improve the machine elements tribological performance [8,9]. Microtextures act as micro-hydrodynamic bearings, enhance load support and increase film thickness, which leads to lower friction compared to untextured surfaces. Lu and Khonsari [10] have presented experimental results concerning the dimples effect on the Stribeck curve. Load, oil type, dimple size, depth and shape were varied to explore their influence on the friction characteristics. By means of the new technology as chemical etching [10], laser surface texturing [11] and novel dressing technique [12], it is now possible to produce controlled micro-geometries (textures) on journal bearing surfaces to enhance the overall tribological performance including friction reduction, reliability improvement, severity of operating conditions, and the energy consumption reduction. Some other and recent studies [13–19] have established that the surface texture geometry such as texture depth, width, textures number, and textures location influence the bearing performance. In recent works, many authors show that the most significant characteristics can be improved through an appropriate arrangement of the textured area on the contact surface [20].

2 Theory

In a hydrodynamic lubrication problem, the governing equations for a full hydrodynamic lubrication region can be described by the known Reynolds' equation. The journal bearing geometry is shown in Figure 1.

[a] Corresponding author: ntalaighil@gmail.com

Nomenclature

a	Circumferential distance between the textures (m)
b	Axial distance between the textures (m)
h	Film thickness (m)
r	Radius of the spherical texture (m)
r_y	Depth of the texture along the radial direction (m)
t	Time (s)
x	Coordinate in circumferential direction (m)
y	Coordinate in radial direction (m)
z	Coordinate in axial direction (m)
C	Radial clearance (m)
F	Applied external load (N)
H	Non-dimensional film thickness [h/C]
$H_{\min}$	Minimum film thickness (m)
L	Bearing length (m)
L/D	Bearing length to diameter ratio
Lx, Lz	Dimensions of the cell containing the texture (m)
N_θ	Number of nodes along circumferential direction
N_Z	Number of nodes along axial direction
Nt_θ	Number of the textures along the circumference of the bearing
Nt_Z	Number of the textures along the length of the bearing
P	Fluid pressure (Pa)
Q	Axial flow ($m^3.s^{-1}$)
R	Bearing radius (m)
T_0	Initial temperature of the fluid (°C)
U_1	Linear velocity of the journal ($m.s^{-1}$)
U_2	Linear velocity of the bearing ($m.s^{-1}$)
W	Supported load (N)
Z	Dimensionless coordinate in axial direction
Z_1, Z_2	Limits of texturation along the axial direction
$\Delta h(\theta, Z)$	Film thickness in the texture (m)
ε	Eccentricity ratio [e/C]
ε_P	Precision for the pressure calculation
ε_W	Precision for the load calculation
ϕ	Attitude angle (°)
μ	Dynamic viscosity of the fluid (Pa.s)
μ_0	Initial viscosity of the fluid (Pa.s)
θ	Angular coordinate (°)
θe	Rupture angle (°)
θ_1, θ_2	Limits of texturation along the circumferential direction (°)
ρ	Fluid density ($kg.m^{-3}$)
ω_1	Rotational speed of the journal (rpm)
ω_2	Rotational speed of the bearing (rpm)
ψ	Applied external force angle (°)
f	Friction coefficient

For Cartesian coordinates, when the thickness of the lubricant film h is in the direction of the y axis (Fig. 2a), the pressure in the lubricating film for a journal operating at steady state, is governed by the following Equation [21]:

$$\frac{\partial}{\partial x}\left(\frac{h^3}{12\mu}\frac{\partial P}{\partial x}\right)+\frac{\partial}{\partial z}\left(\frac{h^3}{12\mu}\frac{\partial P}{\partial z}\right)=\frac{u_2-u_1}{2}\frac{\partial h}{\partial x}+\frac{\partial h}{\partial t} \quad (1)$$

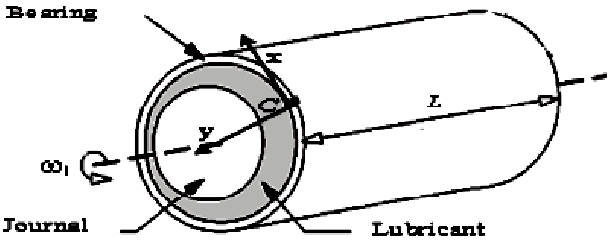

Fig. 1. Hydrodynamic journal bearing geometry.

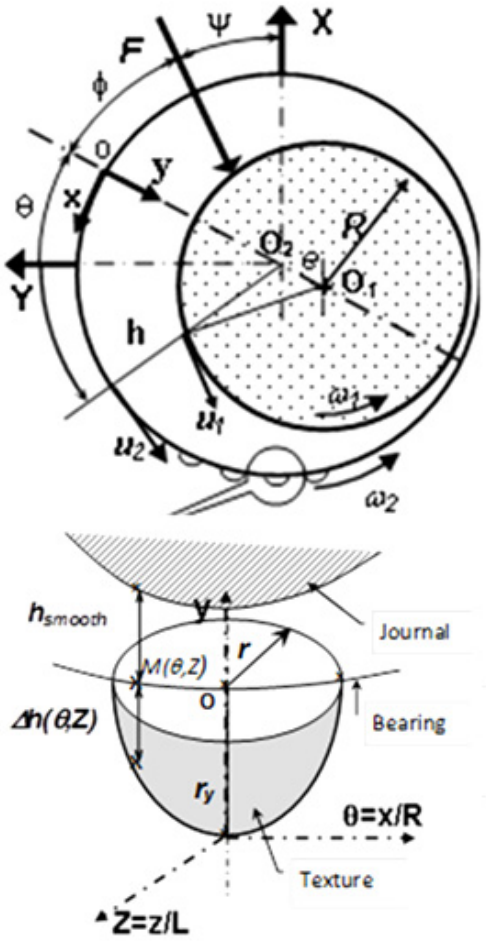

Fig. 2. (a) Right section of the bearing; (b) texture geometry.

P is the lubricant pressure, h is the film height, μ is the dynamic viscosity and u_1, u_2 are the velocities of the journal and the bearing respectively.

When using the variables (Fig. 2b): $Z = z/L$, $\theta = x/R$ and $(u_2 - u_1) = R\,(\omega_2 - \omega_1)$, we have:

$$\frac{\partial}{\partial\theta}\left(h^3\frac{\partial P}{\partial\theta}\right)+\left(\frac{R}{L}\right)^2\frac{\partial}{\partial Z}\left(h^3\frac{\partial P}{\partial Z}\right)=6\mu R^2\left[(\omega_2-\omega_1)\frac{\partial h}{\partial\theta}\right] \quad (2)$$

R is the radius of the journal, L the length of the bearing. ω_1 and ω_2 are respectively, the rotational speeds of the journal and the bearing. h is the film thickness and can be written:

$$h = C\,(1+\varepsilon\cos\theta)+\Delta h\,(\theta, Z) \quad (3)$$

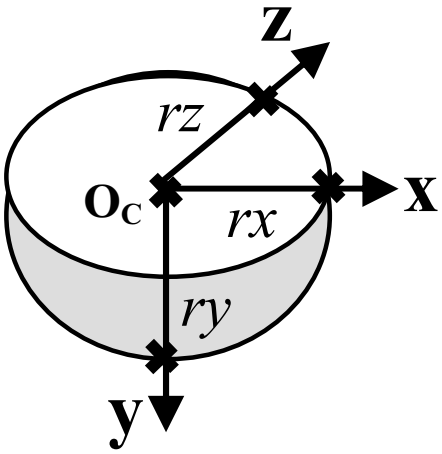

Fig. 3. Texture shape.

In the equation above, $\Delta h(\theta, Z)$ is the film thickness variation due to the textured surface, ε the relative eccentricity of the journal and C the bearing radial clearance.

The boundary conditions, known as Reynolds boundary conditions, are used to determine the film rupture zone. They consist in ensuring that $\partial P/\partial\theta = \partial P/\partial Z = 0$ and $P = 0$ at the rupture limits for the film lubricant defined by the rupture angle θ_e. The bearing is operating under steady state conditions; the applied load F is constant and its direction is vertical ($\psi = 0$). The total load W (supported by the contact) is calculated by integrating the pressure field along the journal bearing surface contact, than the attitude angle ϕ is obtained (Fig. 2a).

Figure 3 shows the texture shape. The texture center is located on the bearing surface, making $y_c = 0$. The depth at point M on the bearing surface situated on the texture geometry is defined by $\Delta h(\theta, Z)$ (Fig. 2b).

The spherical texture geometry is defined by,

$$\frac{(x - x_c)^2}{r^2} + \frac{(\Delta h - y_c)^2}{r_y^2} + \frac{(z - z_c)^2}{r^2} = 1 \qquad (4)$$

In the case of spherical geometry $r_x = r_z = r$, where r is the radius of the circle on the bearing surface. Finally,

$$\Delta h(\theta, Z) = \frac{r_y}{r}\sqrt{r^2 - (x - x_c)^2 - (z - z_c)^2} \qquad (5)$$

3 Problem resolution

The bearing surface is considered stationary and the journal is moving. Only one-half of the journal bearing system is studied due to the bearing symmetry and the use of refined uniform meshes. The used data in our simulations are cited in Table 1.

The imposed precisions for the pressure (P) calculations is $\varepsilon_P = 10^{-7}$ and the load (W) is $\varepsilon_W = 10^{-5}$. The used mesh size is $N_\theta = 929$ and $N_Z = 153$ (one-half of the bearing is meshed). Three configuration cases

Table 1. Geometrical parameters and operating conditions for the studied journal-bearing [10].

External force F (N)	667
Journal speed ω_1 (rpm)	100 to 5000
Shaft diameter (m)	0.024625
Bearing length L (m)	0.0254
Radial clearance C (m)	0.000085
Initial temperature T_0 (°C)	40
Initial viscosity μ_0 (Pa.s)	0.081496
Initial density ρ (kg.m^{-3})	876.3
Mesh: $N_\theta \times N_Z$ (nodes)	929 × 153

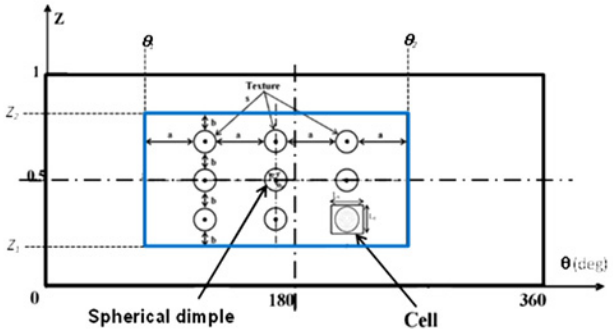

Fig. 4. Textures arrangement on the bearing surface.

are studied: one smooth bearing without texture (Conventional bearing) and two cases of textured bearing (the entire surface of the bearing is textured, from 0 to 360°).

The considered texture geometry in the study is spherical with dimensions:

- Texture 1: diameter of 2 mm and depth r_y = 0.165 mm.
- Texture 2: diameter of 4 mm and depth r_y = 0.448 mm.

Figure 4 shows the textures arrangement on the bearing. θ_1 and θ_2 are the texturation limits along the circumferential direction. Z_1 and Z_2 are the texturation limits along the axial direction. a and b are the distance between the textures along the circumference and along the length of the bearing, respectively. Lx and Lz are the dimensions of the cell containing the texture.

When the bearing is fully textured ($\theta_1 = 0, \theta_2 = 360°$, $Z_1 = 0$ and $Z_2 = 1$), the arrangement for texture 1 is $Nt_\theta = 16$ textures along the circumference and $Nt_Z = 8$ along the length. The arrangement for the texture 2 is $Nt_\theta = 8$ textures along circumference and $Nt_Z = 4$ along the length of the bearing. For the partially textured bearing ($\theta_1 = 185°$, $\theta_2 = 230°$, $Z_1 = 0.12$ and $Z_2 = 0.88$), the arrangement for texture 1 is $Nt_\theta = 4$ textures along the circumference and $Nt_Z = 8$ along the length. The arrangement for the texture 2 is $Nt_\theta = 2$ textures along circumference and $Nt_Z = 4$ along the length of the bearing. Table 2 summarizes the arrangement parameters for the 2 texturation cases.

The pressure field determination in the lubricant film consists in the numerical resolution of Equation (2) by

Table 2. Arrangement parameters for the two cases of texturation.

Parameters	Fully textured		Partially textured	
	Texture 1	Texture 2	Texture 1	Texture 2
$\theta_1 \times \theta_2$ (°)	0×360		185×230	
$Z_1 \times Z_2$	0×1		0.120×0.880	
Dimple diameter (mm)	2	4	2	4
Dimple depth r_y (mm)	0.165	0.448	0.165	0.448
Nt_θ	16	8	4	2
Nt_Z	8	4	8	4
a (mm)	2.668	5.040	0.334	0.557
b (mm)	0.940	1.567	0.635	1.059
Lx (mm)	4.668	9.040	2.334	4.557
Lz (mm)	2.940	5.567	2.635	5.059

using the finite difference method. The best resolution method is that of Christopherson [22] and is considered in this study. The Gauss-Seidel iterative method is used to solve the linear systems obtained after discretization. The use of an iterative method for the resolution is justified by the application of the Reynolds boundary conditions. The analysis leaves the pressure as only unknown to be determined, while the eccentricity is given (e.g. according to the load difference between the given value F and that computed numerically (W) at the previous iteration step). It implies that only Equation (2) is used to form the final equation system for obtaining P, while a cavitation condition should also be satisfied. For a steady-state regime, the computational procedure consists of giving initial values to the eccentricity ε. The pressure field, at each nodal point under a steady external loading F (shown in Fig. 2a) is obtained, fulfilling the pressure convergence condition $|\Delta P_i| / |P_i| \leq \varepsilon_P$.

The supported load W and bearing attitude angle ϕ are then calculated. The calculated load W and applied load F are compared; the process is stopped after the load convergence condition $|F - W| / |F| \leq \varepsilon_W$ is satisfied. If this error control is not satisfied, the eccentricity value is updated and the calculation process begins again.

4 Results and discussions

In this section, the numerical model is validated by comparison with experimental results obtained by Lu and Khonsari [10].

Figure 5 shows a comparison between our numerical results (rotational speed range of 100–5000 rpm) and those obtained experimentally by Lu and Khonsari [10] (rotational speed range of 100–500 rpm). The results of the two studies are in good agreement. The friction coefficient gradually increases with the increase of the journal speed and it varies in the range of 0.001–0.025 as shown in Figure 5a. The case of texture 1 gives a higher friction coefficient (unfavourable case) than the conventional case. A completely textured bearing (from 0 to 360°) with a case of texture 2 gives a low friction coefficient (favourable case) compared to the cases of conventional and texture 1.

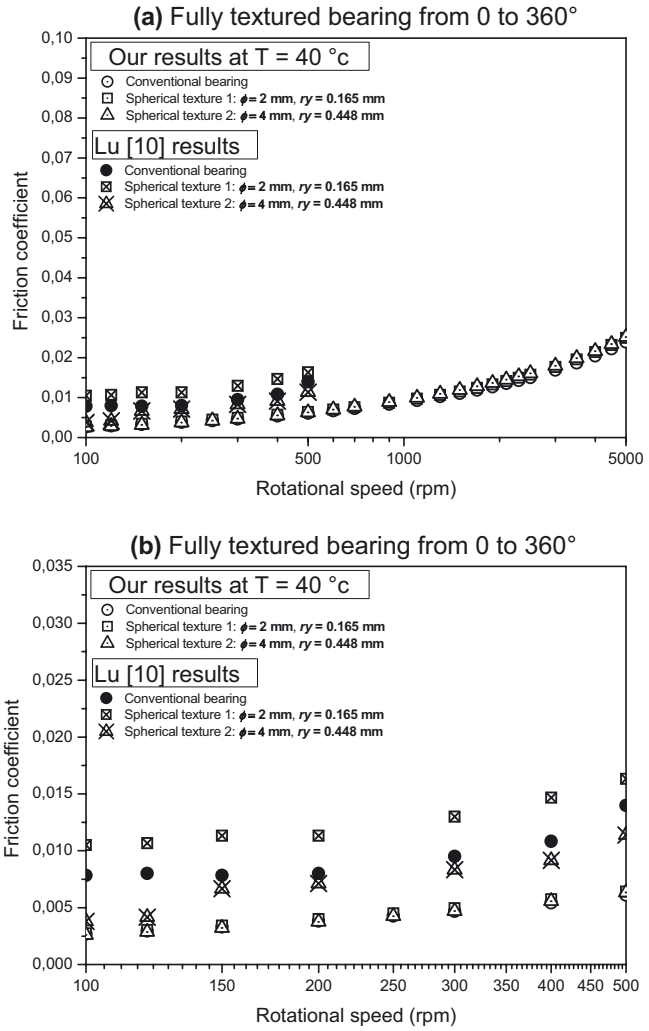

Fig. 5. Friction coefficient as a journal speed function for authors [10] results and our simulation results.

4.1 Pressure field

Figure 6 shows the pressure curve along the median plane of the bearing at $Z = 0.5$ ($z = L/2$) in the case of a contact without textures (conventional) and with textures

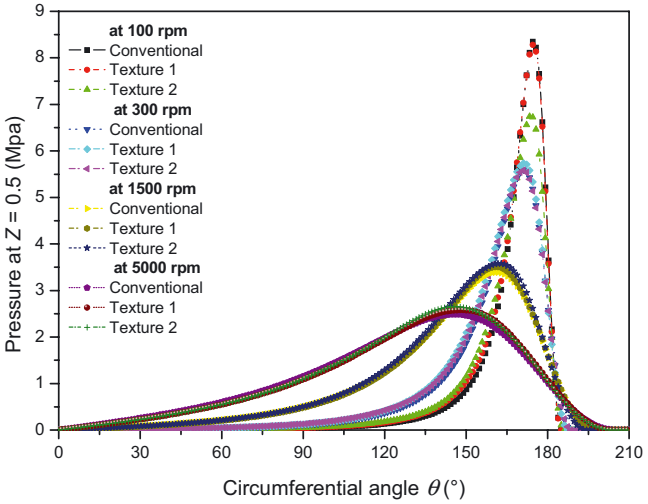

Fig. 6. Profile of the pressure at $Z = 0.5$ with the circumferential angle for four rotational speed values and for fully textured and untextured bearing.

at different rotation speeds (100 rpm, 300 rpm, 1500 rpm and 5000 rpm).

One can notice that the maximum of pressure field decreases with the increase of journal speed. The maximum pressure value of 8.350 MPa is obtained for the lower journal speed (100 rpm). The maximum pressure position moves away from the angular position of 180° with the increase in the journal speed. We also note that above 200 rpm (see Tab. 3); pressure fields obtained for textured and untextured surfaces coincide. For small rotational speeds, the pressure field obtained with the texture 2 is low compared to that obtained with the conventional and texture 1.

From Table 3, we can see that for partially textured bearing surface, the maximum pressure values obtained in the two texturation cases are either equal (up to 300 rpm) or inferior to those of the conventional case. On the other hand, for the fully textured bearing surface case, the maximum pressure values obtained for the texture 1 case are superior to those of conventional case values, except for the texture 2 case where the maximum pressure is lower for journal speeds below 307 rpm.

It is noteworthy to mention that a reduction in the maximum pressure value involves improving the contact characteristics. This is due to the reduction of the cavitation zone (an increase in the rupture angle value).

Figure 7 shows the pressure field evolution in the contact for fully textured and for the three studied cases (conventional bearing, texture 1 and texture 2) at a rotational speed of 300 rpm. The effect of the texture geometry and dimple size on the pressure field shape is very noticeable in particular near the position of 180°.

Figure 8 shows the pressure field evolution in the contact for partially textured (from 185 to 230°) and for the two studied cases (texture 1 and texture 2) at a rotational speed of 300 rpm. The effect of texture geometry and dimple size on the pressure field shape is not easy

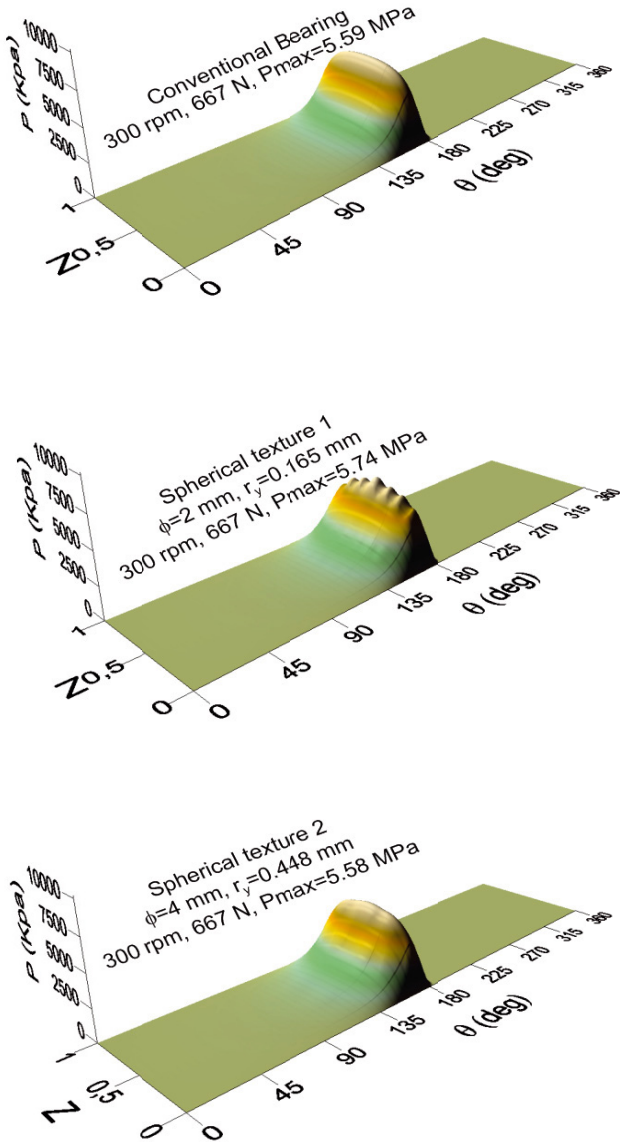

Fig. 7. Evolution of the pressure field for untextured and fully textured surface.

to observe because of the low number of dimples on the bearing surface.

4.2 Contact static parameters

From Figure 9, one can notice that the minimum film thickness, flow rate, friction torque and rupture angle increase with the journal rotational speed. On the other side, the relative eccentricity and the maximum pressure decrease with the journal speed increase.

Compared to the conventional case, we can see that fully texturation does not lead to positive effects, except for small rotational speeds (journal speed below 307 rpm) and only for texturation with texture 2. From the rupture angle and maximum pressure curves, one can conclude that the minimum film thickness improvement and friction coefficient reduction in the case of fully texturing

Table 3. Values of maximum pressure for the three configurations.

Maximum pressure (MPa)					
ω_1 (rpm)	Conventional	Fully textured		Partially textured	
		Texture 1	Texture 2	Texture 1	Texture 2
100	8.350	8.278	6.757	8.350	8.350
120	7.785	7.860	6.544	7.785	7.785
150	7.161	7.338	6.303	7.160	7.161
200	6.448	6.658	6.007	6.441	6.448
250	5.961	6.141	5.776	5.932	5.959
300	5.599	5.738	5.581	5.547	5.584
307	5.558	5.685	5.558	5.504	5.538
400	5.086	5.169	5.256	4.998	5.037
500	4.732	4.791	4.987	4.624	4.656
600	4.466	4.523	4.756	4.354	4.373
700	4.257	4.319	4.555	4.146	4.153
900	3.943	4.023	4.223	3.840	3.827
1100	3.714	3.811	3.959	3.619	3.597
1300	3.537	3.645	3.748	3.448	3.423
1500	3.394	3.511	3.578	3.311	3.286
1700	3.276	3.397	3.440	3.197	3.173
1900	3.176	3.299	3.327	3.101	3.079
2100	3.090	3.213	3.233	3.019	2.999
2300	3.014	3.137	3.154	2.948	2.929
2500	2.948	3.069	3.087	2.885	2.867
3000	2.811	2.926	2.956	2.755	2.742
3500	2.704	2.812	2.856	2.655	2.643
4000	2.617	2.718	2.776	2.574	2.564
4500	2.546	2.641	2.710	2.507	2.498
5000	2.486	2.577	2.653	2.451	2.444

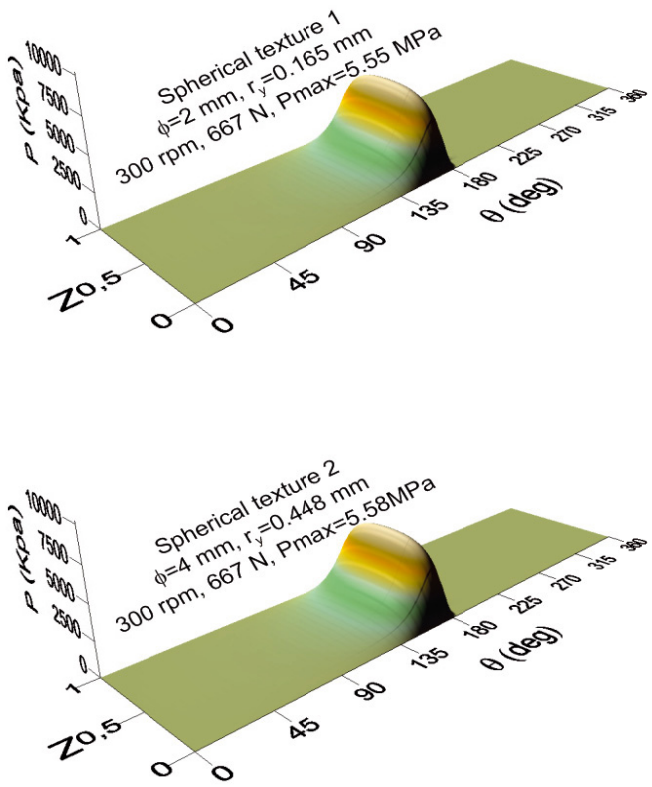

Fig. 8. Evolution of the pressure field for the two cases of partially textured surface.

(texture 2) are rather caused by the reduction of the cavitation zone (thus the increase of the area of active pressure in the lubricating film) than by the contact pressure increase.

From Figure 10, the minimum film thickness, the flow rate, the friction torque and the rupture angle increase with the increase of the journal speed. On the other side, the relative eccentricity and the maximum pressure decrease with the journal speed increase.

In the case of partially textured bearing and compared to the conventional one, one can notice that partially texturation with texture 1 or texture 2, leads to positive effects for all journal speeds values. From the rupture angle curve, an increase of the rupture angle with an increase of the journal speed is observed. When the rupture angle value increases, the lubricating film presence area increases and then the cavitation zone is reduced. In operating steady state and for partially textured bearing surface, the performances of the journal-bearings are slightly improved.

4.3 Film thickness

Figure 11 shows the lubricant film thickness evolution in the contact for fully textured and for the three studied cases (conventional bearing, texture 1 and texture 2) at a rotational speed of 300 rpm.

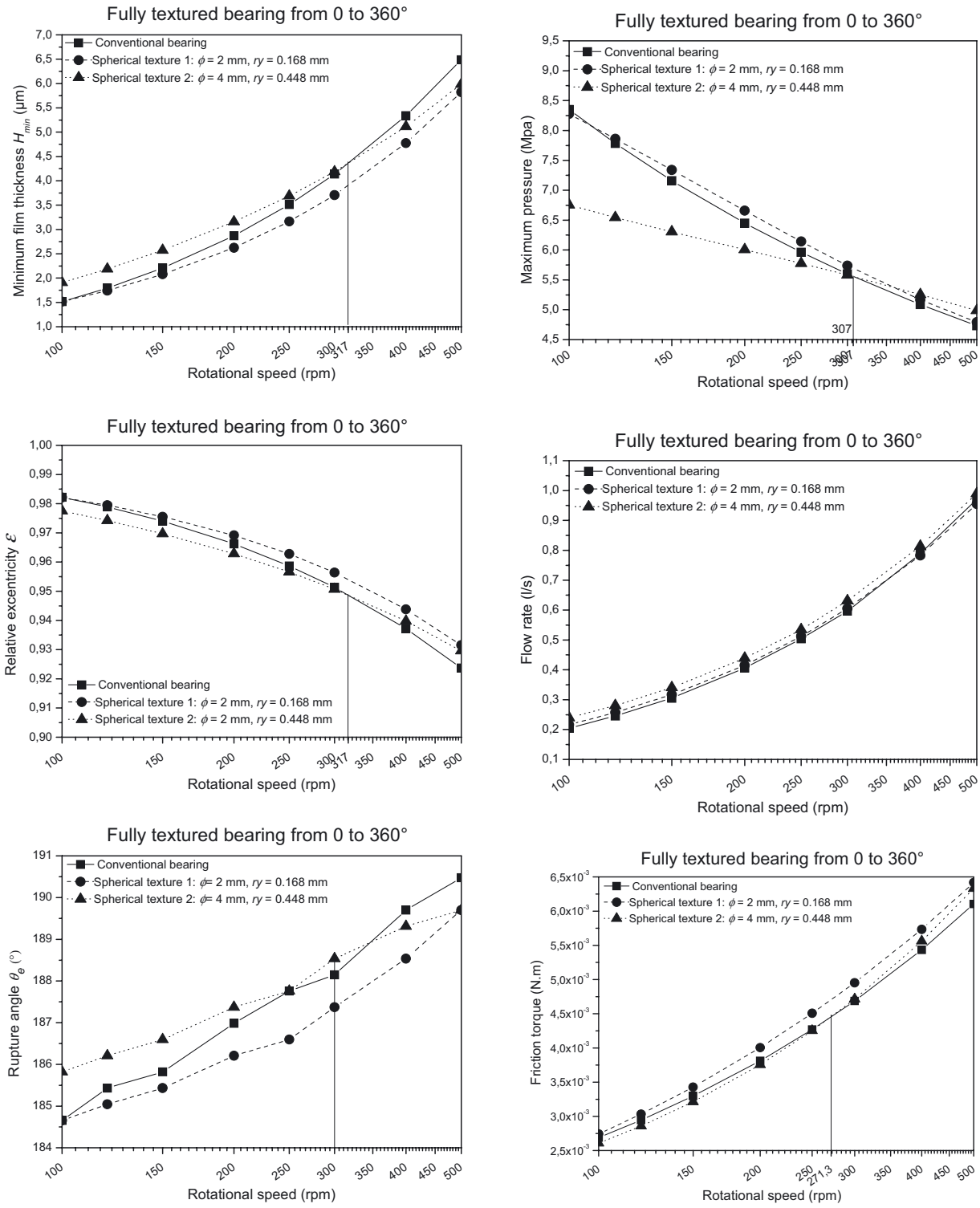

Fig. 9. Evolution of the contact parameters with the rotational speed for fully textured and untextured surface.

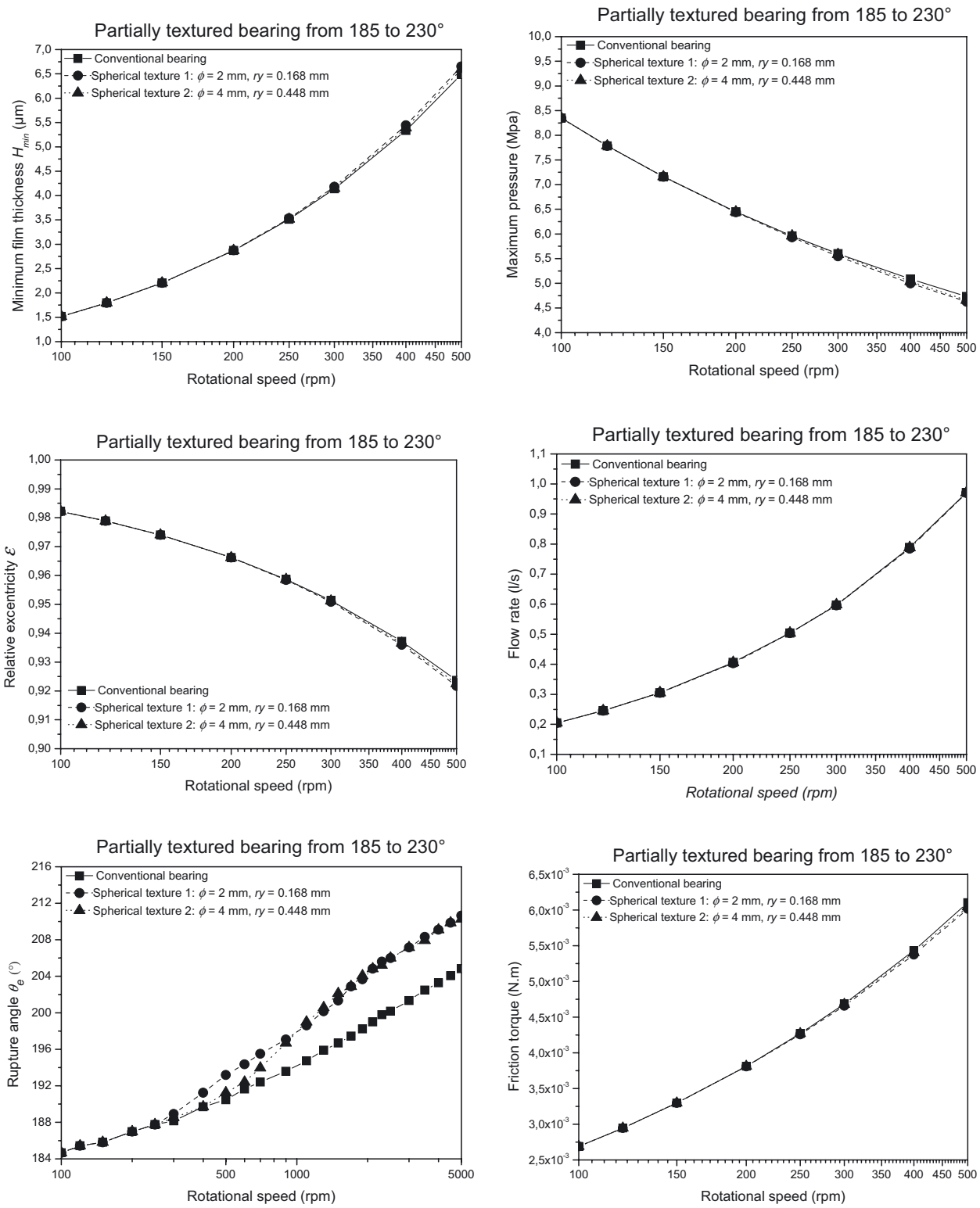

Fig. 10. Evolution of the contact parameters with the rotational speed for partially textured and untextured surface.

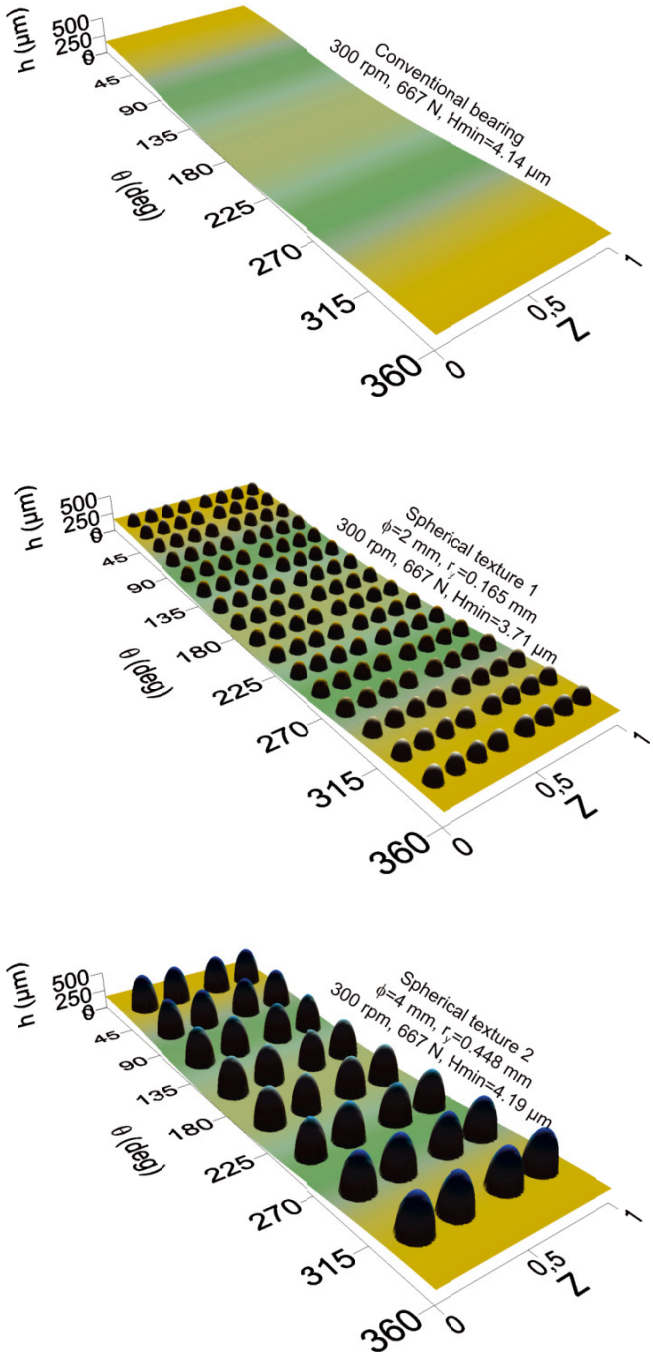

Fig. 11. Evolution of the film thickness for untextured and fully textured surface.

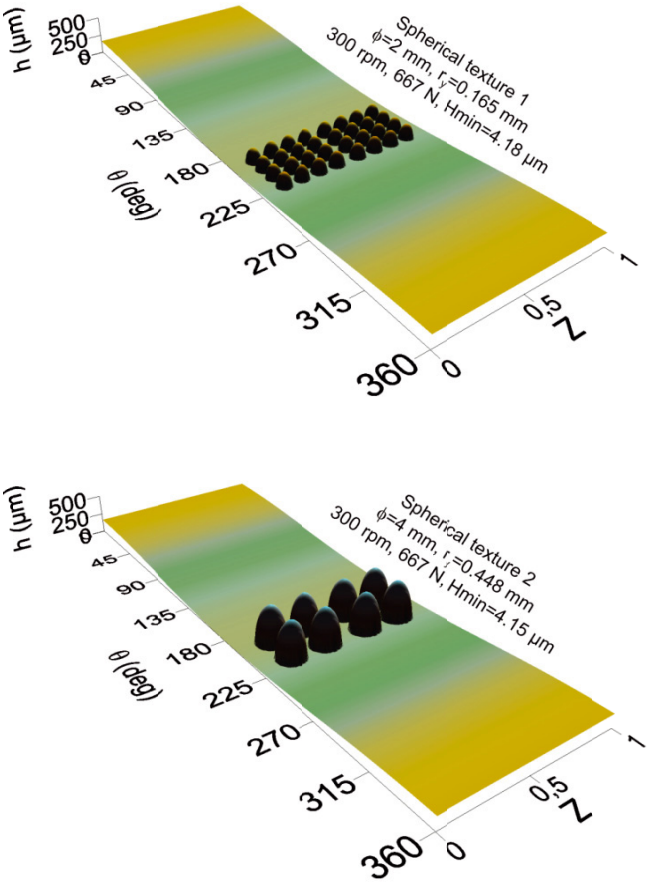

Fig. 12. Evolution of the film thickness for the two cases of partially textured surface.

As is the case for Figure 11, Figure 12 shows the lubricant film thickness evolution in the contact for partially texturing (from 185 to 230°) and for the two studied cases (texture 1 and texture 2) at a rotational speed of 300 rpm.

4.4 Friction coefficient and minimum film thickness

The friction coefficient and the minimum film thickness evolution with the journal speed in the two texturation cases and for fully and partially textured surfaces are shown in Figures 13 and 14, respectively. The friction coefficient and the minimum film thickness increase with the journal speed increase.

Compared to conventional case, partially texturing reduces the friction coefficient for all journal speeds (from 100 to 5000 rpm). Fully texturing raises the friction coefficient value, except for the journal small speeds and in the case of texturation with texture 2.

Compared to conventional case, partially texturing improves the minimum film thickness for all the journal speeds (from 100 to 5000 rpm). Fully texturing reduces the minimum film thickness value, except for the journal small speeds (rotational speed <307 rpm) and in the case of texturation with texture 2.

The relative error evolution between the friction coefficient values obtained for the two textured cases and those obtained for untextured bearing (conventional bearing) with the journal speed are shown in Figure 15. From Figure 15a, we can see that for fully textured bearing and for small rotational speeds (rotational speed <270 rpm); the texture 2 reduces the friction coefficient. At the rotational speed of 100 rpm the friction coefficient is reduced about 3% (the reference value being the friction coefficient obtained for the conventional bearing).

The relative error evolution between the minimum film thickness values obtained for the two textured cases

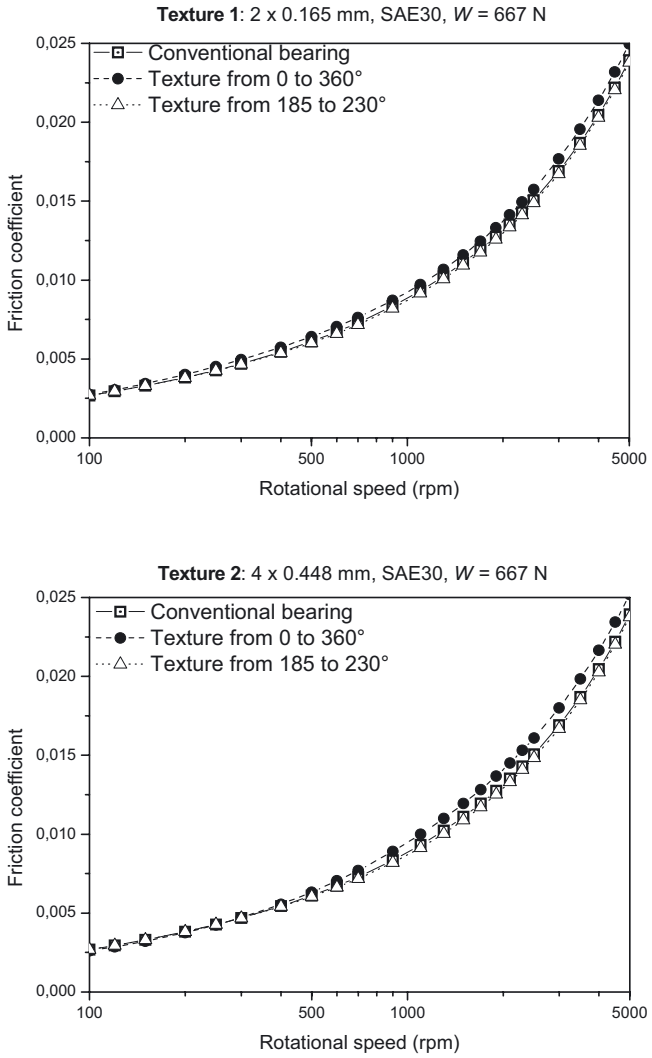

Fig. 13. Evolution of the friction coefficient with the rotational speed in the 2 texturation cases and for fully and partially textured surface.

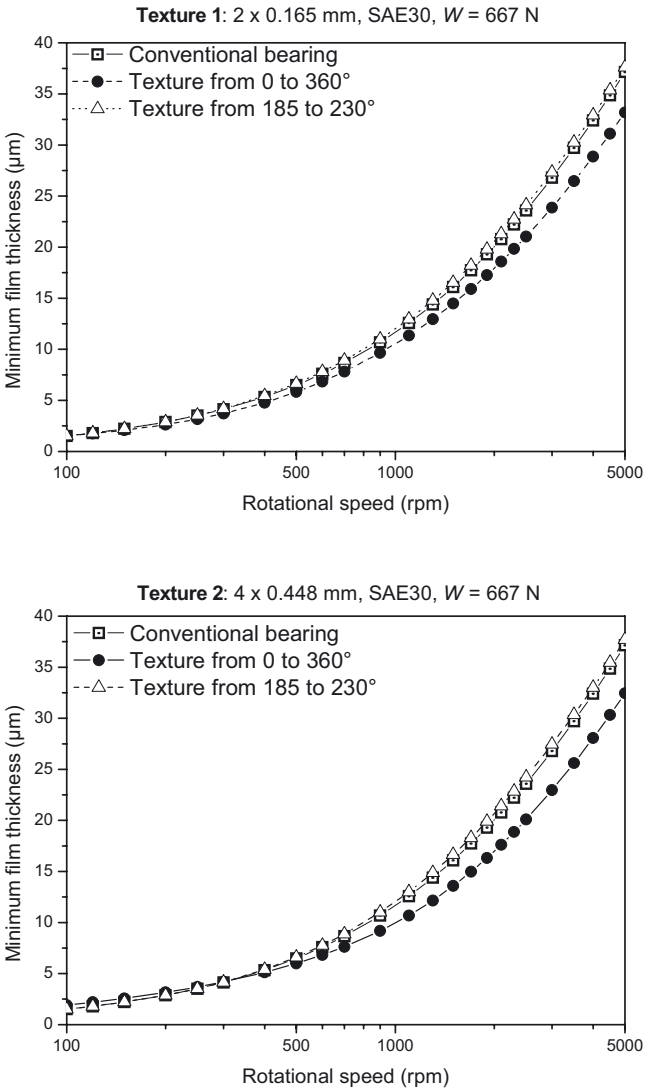

Fig. 14. Evolution of the minimum film thickness with the rotational speed in the 2 texturation cases and for fully and partially textured surface.

and those obtained for untextured bearing (conventional bearing) with the journal speed are shown in Figure 16. From Figure 16a, we can see that for fully textured bearing and for small rotational speeds (rotational speed <318 rpm); the texture 2 improves the minimum film thickness. At a rotational speed equal to 100 rpm, the minimum film thickness is improved by about 27% (the reference value being the minimum film thickness obtained for the conventional bearing).

From Figures 15b and 16b, we can see that for partially textured bearing the friction coefficient and the minimum film thickness are improved for all the journal speeds values. The friction coefficient is reduced about 1.63% at speed of 900 rpm for the texture 1 and about 1.86% at speed of 1300 rpm for the texture 2. The minimum film thickness is raised about 3.0% at speed of 900 rpm for the texture 1 and about 3.4% at speed of 1300 rpm for the texture 2.

5 Conclusion

As a conclusion, it was found that the simulation results obtained in this paper are in good agreement with the litterature experimental results. These are the first significant results, but must be followed by further consideration of the effects of temperature, elastic deformations induced by the thermo-mechanical stresses and the satisfactory cavitation boundary conditions.

- The textures presence over the entire bearing surface does not necessarily improve the hydrodynamic characteristics (friction reduction, increased thickness of the fluid film, improved hydrodynamic lift,...) in a journal bearing contact.
- While for very small journal speeds and adequate texture sizes, fully textured can lead to positive effects.
- Partially textured at the outlet zone has always positive effects.

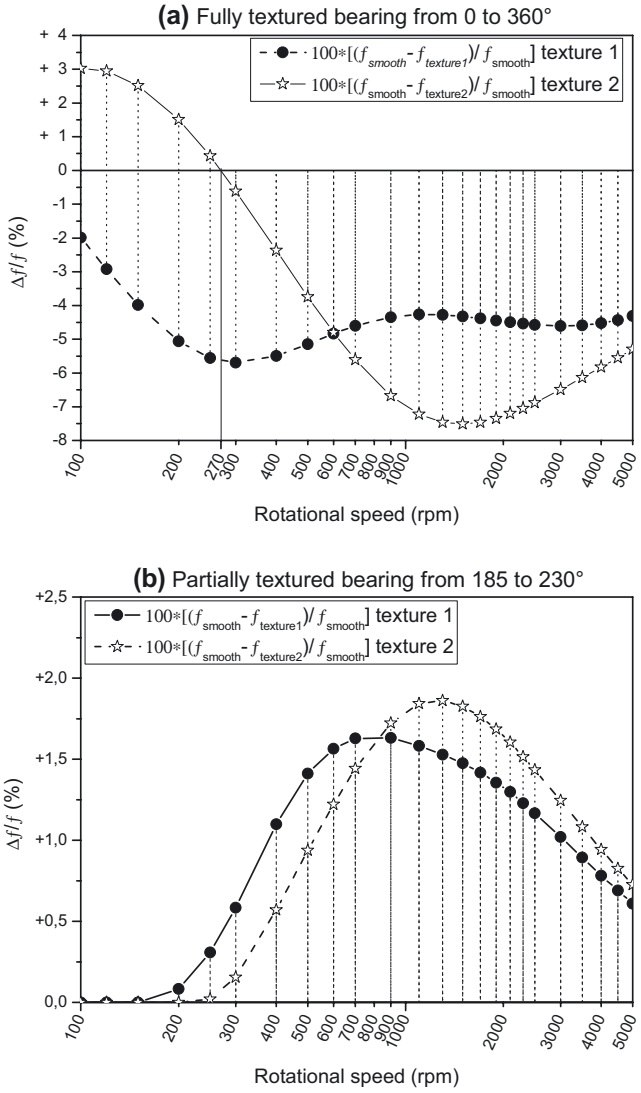

Fig. 15. Evolution of the relative error in the friction coefficient with the journal speed for (a) fully and (b) partially; textured surface.

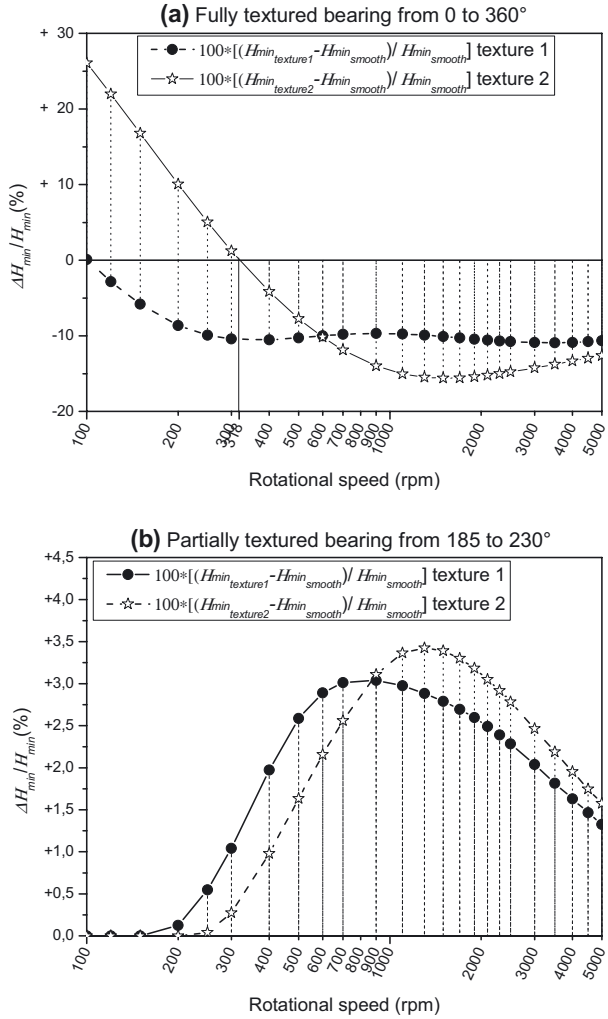

Fig. 16. Evolution of the relative error in the minimum film thickness with the journal speed for (a) fully and (b) partially; textured surface.

– The texture location domain on the bearing is the main criterion for journal bearing performance enhancement.

Finally the journal bearing is a complex system with high film convergence and with cavitation hydrodynamic phenomena. The optimum design of textured area depends strongly on the geometrical parameters and the journal bearing operating conditions.

References

[1] R.A. Mufti, M. Priest, Theoretical and experimental evaluation of engine bearing performance, Proc. Instit. Mech. Eng. Part J: J. Eng. Tribol. 223 (2009) 629–644

[2] A.A. Solghar, S.A. Gandjalikhan Nassab, Thermohydrodynamic behaviors of finite journal bearings with cavitation, Mech. Ind. 12 (2011) 5–15

[3] M.M. Khonsari, E.R. Booser, Applied Tribology: Bearing design and lubrication, John Wiley and Sons, INC, 2001

[4] M. Priest, C.M. Taylor, Automobile engine tribology – approaching the surface, Wear 241 (2000) 193–203

[5] M. Wakuda, Y. Yamauchi, S. Kanzaki, Y. Yasuda, Effect of surface texturing on friction reduction between ceramic and steel materials under lubricated sliding contact, Wear 254 (2003) 356–363

[6] A. Ronen, I. Etsion, Y. Kligerman, Friction-reducing surface-texturing in reciprocating automotive components, Tribol. Trans. 44 (2001) 359–366

[7] A. Ramesh, W. Akram, S.P. Mishra, A.H. Cannon, A.A. Polycarpou, W.P. King, Friction characteristics of microtextured surfaces under mixed and hydrodynamic lubrication, Tribol. Int. 57 (2012) 170–176

[8] I. Etsion, Y. Kligerman, G. Halerin, Analytical and experimental investigation of laser-textured mechanical seal faces, Tribol. Trans. 42 (1999) 511–516

[9] M.D. Pascovici, T. Cicone, M. Fillon, M.B. Dobrica, Analytical investigation of a partially textured parallel slider, Proc. Instit. Mech. Eng. Part J: J. Eng. Tribol. 223 (2009) 151–158

[10] X.B. Lu, M.M. Khonsari, An experimental investigation of dimple effect on the Stribeck curve of journal bearings, Tribol. Lett. 27 (2007) 169–176

[11] I. Etsion, State of the art in laser surface texturing, J. Tribol. 127 (2005) 248–253

[12] J.F.G. Oliveira, A.C. Bottene, T.V. Franca, A novel dressing technique for texturing of ground surfaces, CIRP Ann.-Manufact. Technol. 59 (2010) 361–364

[13] M. Dobrica, M. Fillon, P. Maspeyrot, Mixed EHD, Lubrication in partial journal bearings-comparison between deterministic and stochastic models, ASME J. Tribol. 128 (2006) 778–788

[14] S. Cupillard, S. Glavatskih, M.J. Cervantes, Computational fluid dynamics analysis of journal bearing with surface texturing, Proc. Instit. Mech. Eng. Part J: J. Eng. Tribol. 222 (2008) 97–107

[15] G.C. Buscaglia, I. Ciuperca, M. Jai, The effect of periodic textures on the static characteristics of thrust bearings, J. Tribol. 127 (2005) 899–902

[16] M. Fowel, A.V. Olver, A.D. Gosman, H.A. Spikes, I. Pegg, Entrainment and inlet suction: two mechanisms of hydrodynamic lubrication in textured bearings, J. Tribol. 129 (2007) 336–347

[17] R. Brahamani, A. Shirvani, H. Shirvani, Optimization of partially textured parallel thrust bearings with square-shaped micro-dimples, Tribol. Trans. 50 (2007) 401–406

[18] A.N. Murthy, I. Etsion, F.E. Talke, Analysis of surface textured air bearing sliders with rarefaction effects, Tribol. Lett. 28 (2007) 251–261

[19] N. Tala-ighil, P. Maspeyrot, M. Fillon, A. Bounif, Effects of surface texture on journal bearing characteristics under steady state operating conditions, Proc. Instit. Mech. Eng. Part J: J. Eng. Tribol. 221 (2007) 623–634

[20] N. Tala-Ighil, M. Fillon, P. Maspeyrot, Effect of textured area on the performances of a hyrodynamic journal bearing, Tribol. Int. 44 (2011) 211–219

[21] O. Reynolds, On the theory of lubrication and its application of Mr. Beauchamp Tower's Experiments, Philos. Trans. R Soc. 177 (1886) 157–234

[22] D.G. Christopherson, A new mathematical method for the solution of film lubrication problems, Inst. Mech. Eng. J. Proc. 146 (1941) 126–135